# Combinatorial Investigation of the Effects of the Incorporation of Ti, Si, and Al on the Performance of α-Fe₂O₃ Photoanodes

Jianghua He[†] and B. A. Parkinson[*,‡]

[†]Department of Chemistry, Colorado State University, Fort Collins, Colorado, 80523

[‡]Department of Chemistry and School of Energy Resources, University of Wyoming, Laramie, Wyoming, 82071

ⓢ *Supporting Information*

ABSTRACT: The effect of adding small amounts of Ti, Si, and Al on the photoelectrochemical activity of α-Fe$_2$O$_3$ is investigated using a high-throughput combinatorial method. Quantitative ink jet printing is used to pattern iron oxide and dopant precursors onto conductive glass substrates. Subsequent pyrolysis yields a library of doped iron oxide electrodes that are screened for photoelectrolysis activity by immersing in an electrolyte and scanning a laser over the electrodes to map the photocurrent response. When Si and Al are individually added to iron oxide at the levels we studied, the photoelectrolysis activity decreased whereas low levels of Ti addition enhanced the photocurrents. Synergistic effects were observed resulting in enhanced photocurrents when multiple impurities were added to α-Fe$_2$O$_3$.

KEYWORDS: α-Fe$_2$O$_3$ Photoanodes, Ti, Si, Al, photoelectrochemical activity
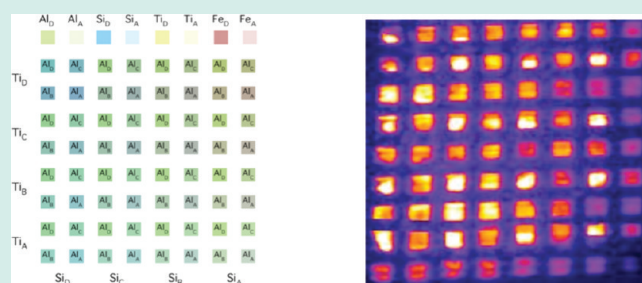
■ INTRODUCTION

Searching for an inexpensive and stable photoanode capable of using visible light to photoelectrolyze water is the topic of much current photoelectrochemical research. Hematite (α-Fe$_2$O$_3$) has received much attention because of its bandgap of 2.2 eV, abundance, nontoxicity, and electrochemical stability. Various synthetic methods have been used to prepare iron oxide photoelectrodes, such as sol–gel, spray pyrolysis, chemical vapor deposition, aqueous self-assembly of nanostrutures, electrochemical deposition, etc.[1−5] However, despite decades of significant research efforts, the efficiency of α-Fe$_2$O$_3$ photoanodes is still very low because of its low absorption coefficient, quite short carrier diffusion lengths and slow electrochemical reaction kinetics. In addition, the conduction band edge of hematite is not negative enough to reduce water to allow spontaneous water splitting meaning that either an applied bias or a second photoelectrode is needed in a photoelectrolysis system.

Many methods have been investigated to improve the photoelectrochemical performance of α-Fe$_2$O$_3$ including the incorporation of various other elements into the hematite films. Grätzel found that the introduction of a small amount of Si into the film dramatically increased the photooxidation current. Many other "dopant" species have also been added including Ca^{2+}, Mg^{2+}, Cu^{2+}, Zn^{2+}, Si^{4+}, Ge^{4+}, Ti^{4+}, Pt^{4+}, Cr^{4+}, V^{5+}, Nb^{5+}, and Mo^{6+}.[6] A number of these elements have improved the photoresponse of α-Fe$_2$O$_3$ but the mechanism for the enhancement has not often been explained. Some reasons for improvements of the photoactivity from adding impurities include lowering the resistivity of the film because of an increase in majority carrier density, improvements in the electrocatalytic activity for water (OH$^-$) oxidation, directing the

morphology of the film (nanostructuring) to allow more carriers to reach the semiconductor/electrolyte interface, passivating grain boundaries, or producing different crystallographic orientations of the α-Fe$_2$O$_3$ crystallites to favor the growth of faces with a lower surface recombination velocity. In addition concentration of impurities at the interface between α-Fe$_2$O$_3$ and the back contact (fluorine doped tin oxide in this study) could also either increase or decrease the photoresponse of the α-Fe$_2$O$_3$ electrode[3,7−9]

The use of the term "dopants", when referring to the addition of more than parts per thousand levels of impurities, does not conform to the usual semiconductor physics definition of electrically active shallow dopants that control the electrical conductivity at the level of parts per million. However since this term has come into wide use, even when adding amounts of elements at levels more properly called solid solutions (if in fact all the additive is incorporated into the lattice), we will continue to use the term "doping" with the understanding that the reason these added elements influence the photocurrent or photovoltage are not usually known.

Given the multitude of possible enhancement effects, adding multiple elemental impurities might result in synergistic effects and produce films with much higher photoactivity than with just one impurity. However given now the large number of possible additives at multiple concentration levels the number of samples that must be prepared becomes very large. The development of combinatorial methods provides tools to speed the discovery and
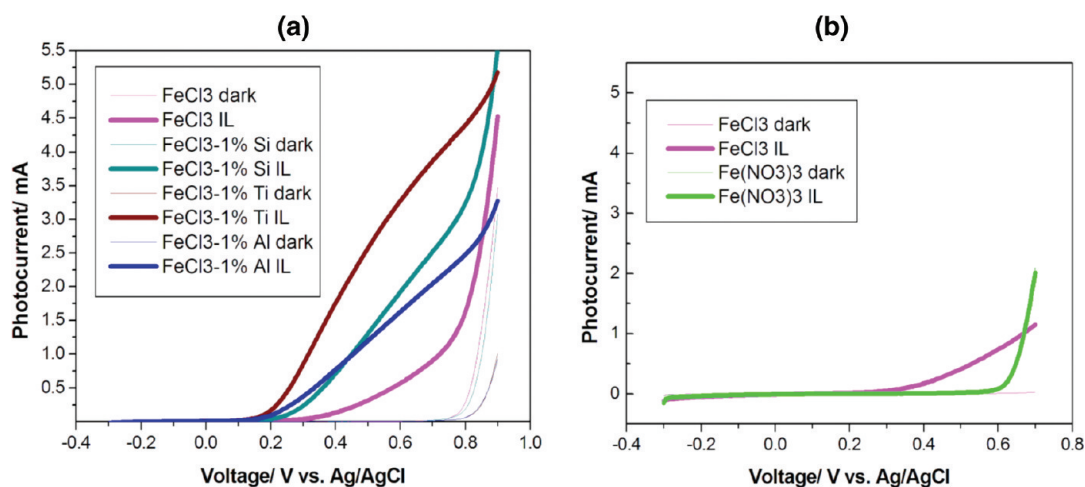
Figure 1. Comparison of $I-V$ curves of (a) undoped Fe_2O_3, Ti-doping, Si-doping, and Al-doping SP thin films irradiated with about a 1 cm^2 spot from a focused 150W Xe arc lamp. (b) Undoped Fe_2O_3 SP thin films obtained from $FeCl_3$ and $Fe(NO_3)_3$. The water oxidation potential in 0.1 M NaOH is about 0.54 V vs Ag/AgCl.

optimization process when a large number of candidate materials need to be synthesized and screened for the property of interest. Recently, our group has developed a simple high-throughput combinatorial search strategy based on ink jet printing to identify multicomponent semiconducting metal oxides with suitable band gaps and band positions for water photoelectrolysis.[10,11] Herein we adapt this technique to quickly produce many "doped" α-Fe_2O_3 compositions and screen them for their water photooxidation activity. We investigate the effects associated with the addition of small amounts of Ti, Si, and Al on the photoelectrochemical performance of the iron oxides, since all of these elements individually have been shown to increase the photoactivity of α-Fe_2O_3.

■ EXPERIMENTAL PROCEDURES

Materials. Precut fluorine-doped tin oxide (FTO) coated glass (TEC 8, 8-ΩR, 75 × 75 × 3 mm) was obtained from Pilkington Industries. Before use the glass was soaked in a piranha solution followed by rinsing with copious amounts of distilled water. $FeCl_3 \cdot 6H_2O$, $Ti(OC_2H_5)_4$, $Si(OC_2H_5)_4$, and $Al(C_3H_5O_2)_3$ were obtained from Sigma Aldrich and used as received.

Preparation and Characterization of Spray Pyrolysis (SP) Thin Film. The SP films were prepared using a commercial artist air brush and a home-built spray pyrolysis system.[12] In our design, cartridge heaters installed into a copper block are used to heat the FTO substrate that is held inside of a square cut out of the top aluminum plate. A thermocouple is also implanted into the block to provide feedback to the temperature controller which controls the temperature as set by the user (herein 370 °C). A solution of 0.5 M $FeCl_3$ in absolute ethanol with or without the addition of Ti, Si, or Al precursors at a 1% stoichiometric ratio was sprayed onto the FTO substrate maintained at 370 °C. The precursor solution was sprayed for ten second intervals and then interrupted until the substrate temperature equilibrated to the set point temperature to ensure complete decomposition of the precursor. Additional layers were applied in the same fashion to obtain the desired film thickness. Usually 6 layers were applied.

Photoelectrochemical (PEC) measurements for SP films were carried out in a standard three-electrode cell using a saturated calomel electrode Ag/AgCl (SCE) reference electrode and a platinum wire as counter electrode. A 1 M NaOH solution was typically used as the electrolyte. It was found that annealing the SP films for 6 h at 500 °C increased the photocurrent dramatically and so this procedure was used for all investigated films. The sample was irradiated with a 150 W Xe arc lamp placed approximately 25 cm from the sample as this was the optimum working distance for focusing the unfiltered light onto the 1 cm ×1 cm area of the sample to obtain the photocurrent—voltage curves.

Preparation and Characterization of Combinatorial Printed Thin Films. The combinatorial templates with defined stoichiometries were printed with a Fujifilm Dimatix model DMP-2800 piezoelectric ink jet printer. A formulation, suitable for the Dimatix inkjet printer, used solutions of the appropriate metal salts (0.50 M for $FeCl_3$, 0.01 M for the other metal precursors) with 35%, by volume, diethylene glycol and 1%, by volume, diethylene glycol monobutyl ether added to serve as the respective roles of viscosity agent and surfactant. In the text these solutions are simply referred to by the metal salt used. The solutions were sonicated for 10 min to ensure complete dissolution and were then injected through a 2 μm syringe filter into empty Fujifilm Dimatix printer cartridges with 10 pL drop volume. Prior to printing, a cleaning cycle was run on each cartridge to ensure that printing was uniform as verified by a print head camera that is built into the printer. The printer also allows for accurate determination of drop volumes, the number of nozzles firing, the piezoelectric jetting waveform for individual nozzles, and the frequency of nozzle firing, all important for a quantitative determination of the amount of each component printed within the combinatorial template. The $FeCl_3$ precursor solutions were overprinted up to three times in order to achieve the optimal metal oxide thickness, while the other metal salts solutions were just printed once.

The substrates with the printed metal precursor patterns were then pyrolyzed in air for approximately 6 h at 500 °C in a ThermoLyne type 1300 furnace to decompose the precursors into metal oxides. Then the printed films were connected as the working electrode to a Princeton Applied Research 174A potentiostat with a platinum basket functioning as both the counter

and reference electrodes in a two-electrode configuration. Since a large area Pt counter electrode was used, and the solution was not deoxygenated, the reference potential (0 V or no bias) corresponds to the oxygen reduction potential in the 0.10 M NaOH solution that was used as the electrolyte. The sample was irradiated with a 532 nm frequency doubled Nd:YAG laser (model LAGR20 from Information Unlimited) with a beam diameter of ~1 mm and a typical illumination intensity of approximately 2500 mW/cm^2. The laser beam was modulated with a PTI OC-4000 chopper operating at 37 Hz and was rastered over the film by applying stepwise voltages to a two-mirror galvanometer (CLS-200 from Intelite, Inc.). The resulting photocurrent at each pixel (generally around 10 μA/cm^2 at short-circuit) was measured using a Stanford Research Systems SR530 model lock-in amplifier. Dark currents across the whole FTO electrode were generally less than 10 nA/cm^2. This photocurrent vs position data was used to generate the false color photocurrent images. Incident photocurrent efficiency (IPCE) values were obtained by dividing the photocurrent by the photon flux of the laser.

■ RESULTS AND DISCUSSION

Figure 1a shows the current—potential ($I-V$) curves of doped and undoped iron oxide films produced by SP in 1 M NaOH solution (pH = 13.6) in the dark and when illuminated. In the dark, the $I-V$ response for all samples is similar and shows no evidence of enhanced electrocatalytic water oxidation due to the dopant. While under illumination, the doped iron oxide thin films show much higher photocurrent than that of undoped sample. Their corresponding iron oxide thin film photoelectrochemical (PEC) performance shows the following order: Ti > Si > Al > no additive. It can also be seen in Figure 1b that different iron salt precursors influence the photocurrent. The PEC performance of iron oxide thin films prepared from FeCl$_3$/EtOH is higher that of thin films prepared from Fe(NO$_3$)$_3$/EtOH. The reasons for this are not investigated in detail however incorporation of carbon from the solvent, nitrogen from the nitrate salt or chloride from FeCl$_3$ could all influence either the electical properties or the morphology of the resulting films. Grätzel's group[8] and others[13] also noticed a strong dependence on photocurrent generation on the identity of the iron precursor and from the presence of impurities. Given that we do not know how these impurities actually increase the photoresponse of the films, we decided to investigate what the synergistic effects of multiple impurity additions on the photoresponse of α-Fe$_2$O$_3$.

With the help of combinatorial method, various rapid screening systems have been developed for discovering and optimizing of potential photocatalysts. The McFarland group has demonstrated the electrochemical deposition of metal oxide compositions using robotics to plate and screen individually created binary oxide materials.[14] The Bard group has developed a screening system for photocatalysts using scanning electrochemical microscopy.[15−18] Recently, our group has developed a new high-throughput combinatorial method for producing and screening metal oxide semiconductors based on ink jet printing of metal oxide precursors. We believe the low-cost, speed, and versatility of ink jet printing make our approach more attractive than other combinatorial search strategies for creating a large variety of compositions in a single experiment and also allowing quantitatively refinement of the composition of photoactive candidates. The high throughput printing step can create 4 or
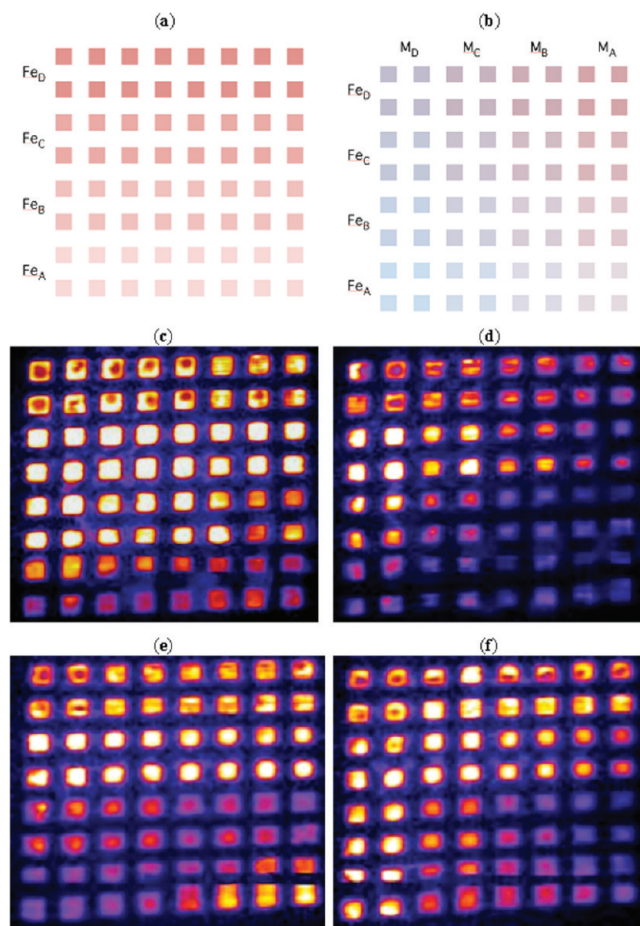
Figure 2. (a) Printing template used for just α-Fe$_2$O$_3$ with ~80 μm drop spacing and double rows printed from the bottom up: once, twice, three times and four times corresponding to Fe$_A$ to Fe$_D$. (b) Printing template used for the Fe−M (M = Ti, Si or Al) series where known amounts of the components are printed on top of the Fe rows from a into individual 3 mm × 3 mm squares resulting in groups of four squares with identical compositions. The density of precursor drops and resulting stoichiometries for d−f are listed in Table 1. False color photocurrent maps of libraries printed using template a (c) α-Fe$_2$O$_3$ and template b (d) Ti-doping; (e) Si-doping; (f) Al-doping. All libraries were scanned at 532 nm with +0.6 bias in a 0.1 M NaOH solution. Note that the false colors are relative within a scan and not absolute values therefore comparisons of color between scans are not quantitative. Refer to Table 2 for more quantitative comparisons.

5 libraries per hour and the laser scanning system can screen a library in about 1 to 2 h under the same conditions to be used in a photoelectrolysis device.

This method can be used not only to search for promising materials capable of the photoelectrolysis of water,[10] but also to optimize their composition[11] and investigate the addition of small amounts of dopants. Since we will be printing arrays of α-Fe$_2$O$_3$ we first optimized the thickness printed films of this material by varying the drop density and the number of times we overprint the pattern. An 8 × 8 array of squares was printed onto SnO$_2$:F-coated glass with 0.5 M FeCl$_3$ with drop spacing of 80 μm. This pattern, shown in Figure 2a, was divided into four double rows printed once, twice, three times, and four times from the bottom to the top, to determine the optimum α-Fe$_2$O$_3$ thickness for the maximum photocurrent signal. It was found that printing

Table 1. Density of Printed Precursor Drops Used to Produce Libraries Shown in Figure 2d−f (Column D to Column A Indicate the Corresponding Stoichiometry of Binary Fe−M System)

| row label	1D DS[a] (μm)	drops per mm^2	relative stoichiometry (Fe$_x$M$_y$)			
			column D	column C	column B	column A
D	40	642	0.0067	0.0017	0.00078	0.00047
C	79	169	0.025	0.0067	0.003	0.0018
B	120	75	0.057	0.015	0.0067	0.004
A	160	45	0.095	0.025	0.011	0.0067

[a] 1D DS = one-dimensional drop spacing.

Table 2. Maximum IPCE Data for Figure 2c−f Measured at Two Different Biases

	undoped Figure 2c	Ti-doped Figure 2d	Si-doped Figure 2e	Al-doped Figure 2f
0 bias	2.60×10^{-4}	4.06×10^{-4}	2.58×10^{-4}	1.85×10^{-4}
+0.6 bias	11.47×10^{-4}	15.54×10^{-4}	7.77×10^{-4}	6.02×10^{-4}

Figure 3. Template used for the printed pattern in the Fe−Ti−Si−Al system where known amounts of the precursors are printed into individual 3 mm × 3 mm squares. The density of precursor drops and resulting stoichiometries for the various produced libraries are listed in Table 3.

this concentration of FeCl$_3$ three times gave the best photocurrent signal (Figure 2c). The top double row (Fe$_D$) was too thick resulting in darker areas in the center of the squares and bright edges due to the film being slightly thinner near the edges. The short diffusion length of carriers in this material results in decreases in photocurrent when the film is too thick. Note that in all cases most of the light still passes through the very thin film of α-Fe$_2$O$_3$, and so incident photon current efficiency (IPCE) values are low.

According to the literature,[9,12,13] the addition of small amounts of Ti, Si or Al improve the photoelectrochemical performance of α-Fe$_2$O$_3$ as was also observed in our above-mentioned SP samples. Therefore we selected Ti, Si, and Al to investigate the effects of the incorporation of small amounts of these elements and combinations of them on thin film α-Fe$_2$O$_3$ photoanodes. We are assuming that addition of these small amounts of impurities does not change the phase from hematite to another iron oxide phase since in previous studies we have anlayzed many iron oxide films produced from these precursors and have always obtained the thermodynamically stable hematite phase under these conditions. Combinatorial printing templates shown in Figure 2a and 2b were created where the total amount of precursor deposited into each square is determined from the concentration of precursor salts in the printing solution, the drop volume of a printed drop, the number of layers printed and the number of drops ink jetted per unit area. This amount is determined by the areal density of dots and the number of inkjetting nozzles actually firing on each printer cartridge. In the pattern, in Figure 2a, four different densities of Fe (increased bottom up) were printed as double horizontal rows. While in Figure 2b, four different densities of Fe (increased from the bottom up) and other metal (M = Ti, Si, or Al) (decreased from left to right) were printed as double horizontal and double vertical rows, respectively resulting in groups of four squares of nominally identical composition. The result of the photocurrent screening is shown in Figure 2d−2f.

Controlling the density of the printed drops allows the production of a quantifiable broad or narrow compositional
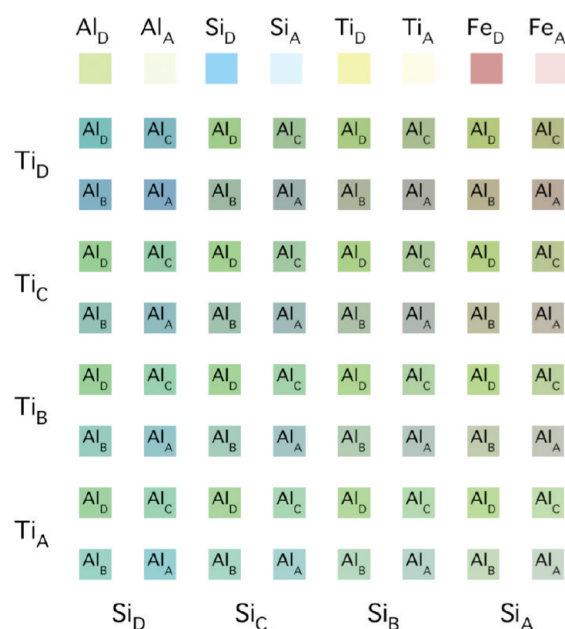
range of dopant additions on each substrate. Table 1 contains the values of the drop spacings and densities used in Figure 2d−f for the Fe and M (M = Ti, Si, or Al) oxide precursors taken individually. For example, the bottom four squares on the far left, corresponding to Fe$_A$M$_D$, were printed with a drop spacing of 160 μm for Fe (three layers) and 40 μm for M (M = Ti, Si, or Al for Figures 2d, e, and f, respectively). This set of squares corresponds to a nominal stoichiometry of Fe$_1$M$_{0.095}$ or 8.7% dopant whereas the smallest percentage square corresponds to Fe$_D$M$_A$ with a nominal stoichiometry of Fe$_1$M$_{0.00047}$ or 0.047% dopant. The corresponding numerical maximum IPCE data are summarized in Table 2. These values can be used to evaluate the relative responses when comparing the false color photocurrent scans since the brightest yellow shade was used to represent the maximum photocurrent response in each image.

We found that in general only Ti-incorporation enhanced the photoelectrochemical performance in comparison with an undoped iron oxide thin film, while the incorporation of Si or Al shows somewhat detrimental effects although there seems to be an increase in response for the thinner iron oxide films with the smallest amount of Si incorporation (Fe$_A$Si$_A$ or Fe$_1$Si$_{0.0067}$, bottom right corner of Figure 2e) suggesting that perhaps even smaller additions of Si might improve the relative photoresponse. In previous work for films prepared by ultrasonic spray pyrolysis the corresponding nominal stoichiometry showing highly improved photoresponse is Fe$_1$Si$_{0.01}$ or ~1% dopant.[12] While our results show detrimental effects from addition of Si at any level when compared to an undoped sample whereas our spray pyrolysis result also shows some improvement with Si incorporation. This may be due to the different methods of producing the films (spray pyrolysis vs ink jet printing) that results in different film morphologies or different amounts of Si incorporation into the films as opposed to forming SiO$_2$. As for the Ti-doped iron oxide thin films, the best photocurrent response was observed at

Table 3. Density of Printed Precursor Drops Used to Produce the Mixtures Shown in Figure 4 (Column 4−7 Corresponds to Figure 4a−d.)a

			relative stoichiometries			
label	1D DS[b] (μm)	drops per mm^2	FeCl$_3$, 3 × DS = 40 μm	FeCl$_3$, 3 × DS = 79 μm	FeCl$_3$, 3 × DS = 120 μm	FeCl$_3$, 3 × DS = 160 μm
D	40	642	0.67%	2.5%	5.7%	9.5%
C	79	169	0.17%	0.67%	1.5%	2.5%
B	120	75	0.078%	0.3%	0.67%	1.1%
A	160	45	0.047%	0.18%	0.49%	0.67%

[a] The iron precursor (FeCl$_3$) was over printed 3 times. [b] 1D DS = one-dimensional drop spacing.
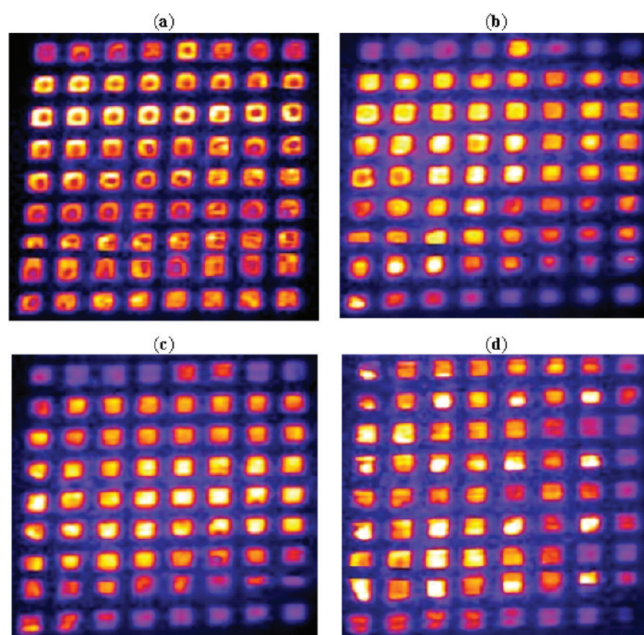
Figure 4. False color photocurrent maps with 532 nm laser excitation of the Fe−Ti−Si−Al system with no applied bias (short circuit) in a 0.1 M NaOH solution (top left FeCl$_3$ precursor drop spacings: a = 40 μm, b = 80 μm, c = 120 μm, d = 160 μm). Note that the false colors are relative within a scan and not absolute values therefore comparisons of color between scans are not quantitative. Refer to Table 4 for quantitative comparisons and the top row of standard squares with only one dopant or no dopant (see text).

the relative stoichiometry of Fe$_1$Ti$_{0.025}$, while it ranges from Fe$_1$Si$_{0.0018}$ (or 0.18% dopant) to Fe$_1$Si$_{0.025}$ (or 2.4% dopant) for Si-doping and Fe$_1$Al$_{0.0067}$ for Al-doping.

There have been numerous reports about the effects on photoelectrochemical response of incorporation of small amounts of the other elements into the binary α-Fe$_2$O$_3$ system. However, it is challenging to investigate the effects of adding multiple elements to α-Fe$_2$O$_3$ thin films especially if individual films have to be prepared at each stoichiometry. Our high-throughput combinatorial method can be used to quickly measure the effects of additions of multiple elements to find an optimal composition. Therefore we printed films with combinations of Ti, Si and Al simultaneously added to α-Fe$_2$O$_3$. A printing template shown in Figure 3 was created where four different densities of Ti, and Si were printed as double horizontal and double vertical rows, respectively and different amounts of Al were deposited in a repeating pattern within groups of four squares containing identical Fe, Ti, and Si amounts. The template was printed four times

Table 4. Summary of Maximum IPCE Data from Figure 4

	4a: DS = 40	4b: DS = 80	4c: DS = 120	4d: DS = 160
0 bias	2.36×10^{-4}	4.52×10^{-4}	4.15×10^{-4}	0.98×10^{-4}
+0.6 V bias	10.16×10^{-4}	15.54×10^{-4}	13.32×10^{-4}	6.26×10^{-4}

with different iron precursor drop spacings. The result is that the total thickness of the α-Fe$_2$O$_3$ decreases from 4a to 4d whereas the relative concentration of the added dopants increases as we make the α-Fe$_2$O$_3$ film thinner. The top row of squares in the template are equal thickness squares of α-Fe$_2$O$_3$ where the first three pairs of squares have only one added metal dopant at the A and D levels (Al, Si, Ti left to right) with the far right pair of squares being just α-Fe$_2$O$_3$ printed at 40 and 160 μm spacings (Fe$_D$ and Fe$_A$). Table 3 contains the values of drop spacings and drop densities used to print the template in Figure 3 for the Fe−Ti−Si−Al oxide precursors. For illustrative purpose, the bottom square on the far left of the template, labeled Si$_D$Ti$_A$Al$_B$, was printed with a drop spacing of 40 μm, 160 μm, and 120 μm for Si, Ti, and Al, respectively, while the Fe precursor was printed in three layers with different drop spacings of 40 μm, 80 μm, 120 μm, 160 μm for Figures 4a to 4d respectively. So this lower left square in Figures 4a to 4d will correspond to stoichiometries of Fe$_1$Si$_{0.0067}$Ti$_{0.00047}$Al$_{0.00078}$, Fe$_1$Si$_{0.025}$Ti$_{0.0018}$Al$_{0.003}$, Fe$_1$Si$_{0.057}$Ti$_{0.0049}$Al$_{0.0067}$ and Fe$_1$Si$_{0.095}$Ti$_{0.0067}$Al$_{0.011}$ respectively. This printing pattern results in libraries of decreasing α-Fe$_2$O$_3$ thickness but increasing doping levels from Figure 4a to 4d. The results of the photocurrent screening of these libraries are shown in Figure 4a to 4d. A series of pairs of internal standards consisting of undoped Fe and the Fe−Ti, Fe−Si and Fe−Al binary systems with different drop densities (thickness) are also printed in the top row of the pattern as seen in Figure 3.

IPCE values from the false color photocurrent data in Figures 4a−d are summarized in Table 4. Again these values can be used to evaluate the relative responses when comparing the false color photocurrent scans since the brightest yellow shade was used to represent the maximum photocurrent response in each image. The highest overall IPCE data was obtained when the FeCl$_3$ precursor was printed three times with a drop spacing of 80 μm followed by drop spacings of 120 μm, 40 and 160 μm (Figures 4b, 4c, 4a, and 4d, respectively). In Figure 4a (FeCl$_3$ DS = 40 μm), the highest IPCE was observed at the Ti-rich area in this pattern (Fe$_1$Ti$_{0.0067}$Si$_x$Al$_x$ top two rows) but the overall thickness of this library was too large for efficient carrier harvesting revealed by the dark squares in the centers of the squares. Figure 4b (DS = 80 μm) has the brightest spots when the relative stoichiometry is near Fe$_1$Ti$_{0.0067}$Si$_{0.0067}$Al$_x$ that occurs in the center section of the library. In Figure 4c (DS = 120 μm) the relative stoichiometry of Fe$_1$Ti$_{0.0017}$Si$_x$Al$_x$ in the second set of double rows appears to have

the highest photocurrent. It is quite interesting to observe there is tendency in Figure 4d for the highest photocurrents appearing in the Al-rich areas with stoichiometry of $Fe_1Ti_xSi_xAl_{0.095}$. Another interesting aspect is that in all of the libraries the pure α-Fe_2O_3 (top right two squares) and the binary internal standards (top row pairs 1−3) almost always have a lower photocurrent response than the ternary additions in their respective libraries. This indicates that there are synergistic effects of adding multiple dopants to the binary oxide semiconductor α-Fe_2O_3. As stated in the introduction this empirical study does not provide information about which of the many possible mechanisms for photocurrent improvement provided by the impurity is actually occurring in the α-Fe_2O_3 film. However it does provide improved stoichiometries that should prove fruitful with more detailed studies of the actual electrical doping, morphological changes, carrier diffusion lengths, and grain boundary and orientation effects attributable to the various impurities.

CONCLUSION

We have confirmed that the photoactivity of α-Fe_2O_3 films produced by spray pyrolysis can be improved by the incorporation of trace amounts of Si, Al or Ti. We then investigated combinations of small amounts of these elements added to α-Fe_2O_3 thin films using a combinatorial technique that uses ink jet printing of metal precursors. Our limited study, using only three added elements with limited ranges of concentrations and concentration ratios in the final films, has only scratched the surface of the possible variations for even this small group of elements, much less exploring synergistic effects from elements that alone may have little or no effect on the photocurrent. Nonetheless, we believe that our approach opens the door for rapid production and screening of many combinations of added dopants that will eventually result in bulk and added impurity compositions that can efficiently photoelectrolyze water in an inexpensive thin film device.

ASSOCIATED CONTENT

ⓢ Supporting Information. Additional information and references. This material is available free of charge via the Internet at http://pubs.acs.org.

AUTHOR INFORMATION

Corresponding Author
*E-mail: bparkin1@uwyo.edu.

ACKNOWLEDGMENT

REFERENCES

(1) Gash, A. E.; Tillotson, T. M.; Satcher, J. H.; Poco, J. F.; Hrubesh, L. W.; Simpson, R. L. Use of Epoxides in the Sol−Gel Synthesis of Porous Iron(III) Oxide Monoliths from Fe(III) Salts. *Chem. Mater.* **2001**, *13*, 999–1007.

(2) Ingler, W. B.; Baltrus, J. P.; Khan, S. U. M. Photoresponse of p-Type Zinc-Doped Iron(III) Oxide Thin Films. *J. Am. Chem. Soc.* **2004**, *126*, 10238–10239.

(3) Kay, A.; Cesar, I.; Gratzel, M. New Benchmark for Water Photooxidation by Nanostructured α-Fe_2O_3 Films. *J. Am. Chem. Soc.* **2006**, *128*, 15714–15721.

(4) Vayssieres, L.; Guo, J. H.; Nordgren, J. Aqueous Chemical Growth of α-Fe_2O_3−α-Cr_2O_3 Nanocomposite Thin Films. *J. Nanosci. Nanotechnol.* **2001**, *1*, 385–388.

(5) Hu, Y.-S.; Kleiman-Shwarscstein, A.; Forman, A.; Park, J.-N.; McFarland, E. W. *Chem. Mater.* **2008**, *20*, 3803 Many other synthetic methods exist; see Supporting Information for additional references.

(6) Additional literature about the influence of different "dopant" species are listed in the Supporting Information.

(7) Duret, A.; Gratzel, M. Visible Light-Induced Water Oxidation on Mesoscopic α-Fe2O3 Films Made by Ultrasonic Spray Pyrolysis. *J. Phys. Chem. B* **2005**, *109*, 17184.

(8) Cesar, I.; Kay, A.; Cesar, I.; Martinez, J. A. G.; Grätzel, M. Translucent Thin Film Fe_2O_3 Photoanodes for Efficient Water Splitting by Sunlight: Nanostructure-Directing Effect of Si-Doping. *J. Am. Chem. Soc.* **2006**, *128*, 4582–4583.

(9) Glasscock, J. A.; Barnes, P. R. F.; Plumb, I. C.; Savvides, N. Enhancement of Photoelectrochemical Hydrogen Production from Hematite Thin Films by the Introduction of Ti and Si. *J. Phys. Chem. C* **2007**, *111*, 16477–16488.

(10) Woodhouse, M.; Herman, G. S.; Parkinson, B. A. Combinatorial Approach to Identification of Catalysts for the Photoelectrolysis of Water. *Chem. Mater.* **2005**, *17*, 4318.

(11) Woodhouse, M.; Parkinson, B. A. Combinatorial Discovery and Optimization of a Complex Oxide with Water Photoelectrolysis Activity. *Chem. Mater.* **2008**, *20*, 2495–2502.

(12) Woodhouse, M., Doctoral Dissertation, Department of Chemistry, Colorado State University . 2007.

(13) Sartoretti, C. J.; Alexander, B. D.; Solarska, R.; Rutkowska, W. A.; Augustynski, J.; Cerny, R. Photoelectrochemical Oxidation of Water at Transparent Ferric Oxide Film Electrodes. *J. Phys. Chem. B* **2005**, *109*, 13685–13692.

(14) Baeck, S. H.; Jaramillo, T. F.; Brandli, C.; McFarland, E. W. Combinatorial Electrochemical Synthesis and Characterization of Tungsten-Based Mixed-Metal Oxides. *J. Comb. Chem.* **2002**, *4*, 563–568.

(15) Lee, J.; Ye, H. C.; Pan, S. L.; Bard, A. J. Screening of Photocatalysts by Scanning Electrochemical Microscopy. *Anal. Chem.* **2008**, *80*, 7445–7450.

(16) Jang, J. S.; Yoon, K. Y.; Xiao, X. Y.; Fan, F. F.; Bard, A. J. Development of a Potential Fe_2O_3-Based Photocatalyst Thin Film for Water Oxidation by Scanning Electrochemical Microscopy: Effects of Ag-Fe_2O_3 Nanocomposite and Sn Doping. *Chem. Mater.* **2009**, *21*, 4803–4810.

(17) Jang, J. S.; Lee, J. W.; Xiao, X. Y.; Fan, F. F.; Bard, A. J. Rapid Screening of Effective Dopants for Fe_2O_3 Photocatalysts with Scanning Electrochemical Microscopy and Investigation of Their Photoelectrochemical Properties. *J. Phys. Chem. C* **2009**, *113*, 6719–6724.

(18) Liu, W.; Ye, H. C.; Bard, A. J. Screening of Novel Metal Oxide Photocatalysts by Scanning Electrochemical Microscopy and Research of Their Photoelectrochemical Properties. *J. Phys. Chem. C* **2010**, *114*, 1201–1207.